

The $\Sigma - D$ relation for planetary nebulae

D. Urošević^{1,5}, B. Vukotić², B. Arbutina¹, D. Ilić^{1,5}, M. Filipović³, I. Bojičić⁴, S. Šegan¹, and S. Vidojević¹

¹ Department of Astronomy, Faculty of Mathematics, University of Belgrade, Studentski trg 16, P.O. 550, 11000 Belgrade, Serbia

² Astronomical Observatory, Volgina 7, 11160 Belgrade 74, Serbia

³ University of Western Sydney, Locked Bag 1797, Penrith South DC, NSW 1797, Australia

⁴ Department of Physics, Macquarie University, Sydney, NSW 2109, Australia

⁵ Isaac Newton Institute of Chile, Yugoslavia Branch

Abstract. We present an extended analysis of the relation between radio surface brightness and diameter – the so-called $\Sigma - D$ relation for planetary nebulae (PNe). We revise our previous derivation of the theoretical $\Sigma - D$ relation for the evolution of bremsstrahlung surface brightness in order to include the influence of the fast wind from the central star. Different theoretical forms are derived: $\Sigma \propto D^{-1}$ for the first and second phases of evolution and $\Sigma \propto D^{-3}$ for the final stage of evolution. Also, we analyzed several different Galactic PN samples. All samples are influenced by severe selection effects, but Malmquist bias seems to be less influential here than in the supernova remnant (SNR) samples. We derived empirical $\Sigma - D$ relations for 27 sample sets using 6 updated PN papers from which an additional 21 new sets were extracted. Twenty four of these have a trivial form of $\beta \approx 2$. However, we obtain one empirical $\Sigma - D$ relation that may be useful for determining distances to PNe. This relation is obtained by extracting a recent nearby (< 1 kpc) Galactic PN sample.

Key words. planetary nebulae: general – radio continuum: ISM – methods: analytical – methods: statistical – ISM: supernova remnants

1. Introduction

Planetary nebulae (PNe) are usually identified by their optical spectra, consisting mainly of recombination lines of hydrogen, helium and collisionally excited light elements. They are composed of gaseous shells ionized by a hot central star, which allow for the necessary conditions to create their spectra. PNe were first discovered over 200 years ago. Today, there are more than 2500 confirmed Galactic PNe with total number estimates at least ten times higher. PNe emission from radio to X-ray have been detected over the past 30 years. Several hundreds of these PNe have been observed in radio-continuum alone. Their number far out-rank the known Galactic supernova remnant (SNR) population (approximately 250).

The relation between radio surface brightness and diameter for SNRs, the so-called $\Sigma - D$ relation, has been the subject of extensive discussions over the past forty years. This $\Sigma - D$ relation has a power law form:

$$\Sigma \propto D^{-\beta}, \quad (1)$$

where Σ is the radio surface brightness, D is diameter and β the slope of the log-log plot.

Observational improvements, including the increased use of radio interferometers, account for the high number of resolved radio PNe over the past two decades. The $\Sigma - D$ relation for PNe has only been sporadically discussed (for example, Amnuel et al. 1984) until Urošević et al. (2007) (hereafter Paper I).

The statistical analysis of the Galactic PN distances was presented in Daub (1982) and in Cahn, Kaler & Stanghellini (1992). Using radio data, the primary statistical method for determining distance was based on the correlation between PN radius and brightness temperature, known as the $R - T_b$ relation¹. Van de Steene & Zijlstra (1995) derived an empirical $R - T_b$ relation for 131 Galactic PNe, felt to be located near the Galactic center, at approximately the same distance. Additionally, a smaller sample of 23 (non-Galactic bulge) PNe were studied having well-determined distances. The same calibration relations were obtained in both cases. Zhang (1995) studied the statistical distance scale for PNe based on another sample of 132 PNe having well-determined individual distances. He found that the derived distance scale was in good agreement with those derived by Van de Steene & Zijlstra (1995). More

Send offprint requests to: Dejan Urošević, e-mail: dejanu@matf.bg.ac.yu

¹ This relation is essentially equivalent to the $D - \Sigma$ relation.

recently, Phillips (2002) (hereafter Ph02) derived $R - T_b$ relations for 44 nearby PNe whose distances are less than 0.7 kpc. Thus, different samples of Galactic PNe with known distances were defined in the three previously cited papers. All of these derived $R - T_b$ relations were applied to PNe with unknown distances. We also note that a recent paper by Stanghellini, Shaw & Villaver (2008) (hereafter SSV) gives an updated reliable sample of individual Galactic PN distances.

The statistical analysis of Galactic radio PNe is less developed than those of Galactic SNRs². Therefore, selection effects are felt to greatly influence Galactic radio PN samples causing the statistical determination of distance to be highly uncertain.

In the present paper, we use the methodology for the statistical analysis of SNRs to improve that for Galactic radio PNe. Primary objectives include the following:

- (i) Development of an improved form of the theoretical $\Sigma - D$ relation for PNe (compared to the one derived in Paper I) by incorporating the interaction between asymptotic-giant-branch (AGB) star wind and the fast wind from the central star.
- (ii) Derivation of improved empirical $\Sigma - D$ relations using current and previous samples to determine if these are all under the influence of selection effects.
- (iii) Validation of $\Sigma - D$ relations for the determination of radio PN distance.

2. Dynamics of PNe

In considering the dynamics of PNe, we adopt the *interacting stellar winds model* (ISW; Zhang & Kwok 1993, Kwok 1994, and references therein). This model implies that a nebular shell results from the sweeping up of circumstellar material moving within the AGB star wind by a fast wind emanating from the PN central star. The speed of the fast wind is 100 times that of the AGB wind and acts as a "snowplow", piling up matter into a high density shell. This interaction produces two shocks. The inner shock is formed at the interaction between central star wind and shell. The outer one is situated in the AGB wind just outside the shell. Most of the volume interior of the shell is made up of shocked central-star wind at a high temperature (millions of degrees). The outer shock is likely to be isothermal – similar to the shocks in the radiative phase of SNR evolution, where a dense shell is formed.

The dependence between gas density and radius of a PN is necessary for deriving the theoretical $\Sigma - D$ relation for PNe. This dependence was shown in Paper I for a model consisting of one steady wind emanating from the central star. A trend of decreasing radio surface brightness with increasing diameter was shown in Paper I. The

² The radio samples of Galactic PNe are richer in terms of the number of objects, but incompleteness is drastically higher than in SNR samples – less than 5% of total number of PNe can be detected by radio surveys (Kwok 1994).

radiation mechanism used for derivation of the theoretical $\Sigma - D$ relation is thermal bremsstrahlung, which is the basic process of radio-continuum emission in H II regions.

We begin our derivation using the following notation:

R_s – shell radius,

R_o – outer radius of the shell,

R_i – inner radius of the shell,

V_s – velocity of the shell,

V – AGB wind velocity,

v – fast wind velocity,

\dot{M} – mass loss in the AGB phase,

\dot{m} – fast wind mass loss,

M_s – mass in the shell,

ρ_s – density of the shell,

$t = 0$ – the moment when the AGB wind stops,

$t = \tau$ – the moment when the fast wind starts.

2.1. The momentum conserving phase

If we assume momentum conservation during the interaction, then:

$$P_s = M_s V_s = P_{AGB} + P_{FW}, \quad (2)$$

$$\begin{aligned} P_s &= P_{AGB} + P_{FW} \\ &= \int_{Vt}^{R_o} 4\pi r^2 \rho_{AGB} V dr + \int_{R_i}^{v(t-\tau)} 4\pi r^2 \rho_{FW} v dr \\ &= \int_{Vt}^{R_o} 4\pi r^2 \frac{\dot{M}}{4\pi r^2 V} V dr + \int_{R_i}^{v(t-\tau)} 4\pi r^2 \frac{\dot{m}}{4\pi r^2 v} v dr \\ &= \dot{M}(R_o - Vt) + \dot{m}(v(t - \tau) - R_i), \end{aligned} \quad (3)$$

while the mass in the shell is:

$$\begin{aligned} M_s &= M_{AGB} + M_{FW} \\ &= \int_{Vt}^{R_o} 4\pi r^2 \rho_{AGB} dr + \int_{R_i}^{v(t-\tau)} 4\pi r^2 \rho_{FW} dr \\ &= \int_{Vt}^{R_o} 4\pi r^2 \frac{\dot{M}}{4\pi r^2 V} dr + \int_{R_i}^{v(t-\tau)} 4\pi r^2 \frac{\dot{m}}{4\pi r^2 v} dr \\ &= \frac{\dot{M}}{V}(R_o - Vt) + \frac{\dot{m}}{v}(v(t - \tau) - R_i). \end{aligned} \quad (4)$$

If, additionally, the shell is thin: $R_i \rightarrow R_o = R_s$ then we may write:

$$P_s = (\dot{M} - \dot{m})R_s - \dot{M}Vt + \dot{m}v(t - \tau), \quad (5)$$

$$M_s = \left(\frac{\dot{M}}{V} - \frac{\dot{m}}{v}\right)R_s - \dot{M}t + \dot{m}(t - \tau) \quad (6)$$

(see Equation 6 in Zhang & Kwok 1993).

If $V_s = \text{const.}$, the shell is expanding following the law:

$$R_s = \frac{vV\tau}{v - V} + V_s\left(t - \frac{v\tau}{v - V}\right), \quad (7)$$

which may be reduced to Equation (5) in Zhang & Kwok (1993) if $v \gg V$:

$$R_s \approx V\tau + V_s(t - \tau). \quad (8)$$

If $t \gg \tau$ then,

$$R_s \approx V_s t, \quad (9)$$

and the shell velocity can be expressed as:

$$V_s = \frac{P_s}{M_s} = \frac{(\dot{M} - \dot{m})R_s + (\dot{m}v - \dot{M}V)\frac{R_s}{V_s}}{\left(\frac{\dot{M}}{V} - \frac{\dot{m}}{v}\right)R_s + (\dot{m} - \dot{M})\frac{R_s}{V_s}}. \quad (10)$$

Solving this equation we obtain:

$$V_s = \frac{\dot{M} - \dot{m} + (v - V)\sqrt{\frac{\dot{M}\dot{m}}{vV}}}{\frac{\dot{M}}{V} - \frac{\dot{m}}{v}}, \quad (11)$$

which is Equation (4) in Zhang & Kwok (1993).

The average density inside the shell can be expressed as:

$$\rho_s = \frac{M_s}{\frac{4\pi}{3}fR_s^3}, \quad (12)$$

where f is the volume filling factor. From Equations (6) and (9) we see that if $t \gg \tau$:

$$M_s = \left[\left(\frac{\dot{M}}{V} - \frac{\dot{m}}{v}\right) + \frac{\dot{m} - \dot{M}}{V_s}\right]R_s. \quad (13)$$

If $\dot{M} \gg \dot{m}$, and $v \gg V$, then $M_s \approx \left(\frac{\dot{M}}{V} + \frac{\dot{m} - \dot{M}}{V_s}\right)R_s$ and

$$\rho_s \propto \frac{\dot{M}}{4\pi R_s^2 V}. \quad (14)$$

Essentially, we have perturbed the AGB wind ($\rho_{AGB} = \frac{\dot{M}}{4\pi R_{AGB}^2 V}$). From Equation (11) we estimate $V_s \approx 15 \text{ km s}^{-1}$ using typical values of $\dot{M} = 10^{-5} M_\odot \text{ yr}^{-1}$, $\dot{m} = 10^{-8} M_\odot \text{ yr}^{-1}$, $V = 10 \text{ km s}^{-1}$ and $v = 2000 \text{ km s}^{-1}$. We obtain the dependence $\rho_s \propto R_s^{-1}$ using Equations (12) and (13) assuming that the shell thickness $\Delta = R_o - R_i = \text{const.}$ and $f = 1 - \left(\frac{R_i}{R_o}\right)^3 = 1 - \left(1 - \frac{\Delta}{R_s}\right)^3 \approx 3\Delta/R_s$.

2.2. The energy conserving phase

The momentum-conserving phase is perhaps, a reasonable description of early PN evolution. However, if a part of the energy of the fast wind is transformed into thermal energy, then the pressure of the hot bubble (P) will provide additional acceleration to the nebular shell. In this ‘‘energy-conserving’’ phase, the equation of motion and the energy equation is expressed as:

$$M_s \frac{d^2 R_s}{dt^2} = 4\pi R_s^2 P - \frac{\dot{M}}{V}(V_s - V)^2, \quad (15)$$

$$\frac{d}{dt}\left(\frac{1}{\gamma - 1}P \cdot \frac{4\pi}{3}R_s^3\right) = \frac{1}{2}\dot{m}v^2 - 4\pi R_s^2 P V_s \quad (16)$$

(Kwok 2000).

The similarity solution method can be used for defining the change of PN radius with time. The power-law form $R_s \propto t^\alpha$, is expected for a PN in the energy conserving phase of evolution. We can define dimensionless variable in form:

$$\xi \equiv R_s t^l \rho_{AGB}^m \dot{E}^n, \quad (17)$$

where \dot{E} is the power of fast wind which injects energy (through the inner shock) into the hot bubble. After similarity analysis, the following expression is obtained:

$$R_s = \xi \left(\frac{\dot{E}}{\rho_{AGB}}\right)^{\frac{1}{5}} t^{\frac{3}{5}}. \quad (18)$$

We obtain a $R_s \propto t$ ($\alpha = 1$) dependence assuming $\rho_{AGB} \propto R_s^{-2}$ and using Equation (18). Finally, a stationary solution $V_s = \dot{R}_s = \text{const.}$ can be used for further derivations.

The mass of the compressed AGB wind in the shell, using $V_s = \text{const.}$, is:

$$M_s = \dot{M} \left(\frac{1}{V} - \frac{1}{V_s}\right) R_s. \quad (19)$$

If for f , we assume $\Delta = \text{const.}$, then Equation (12) implies $\rho_s \propto R_s^{-1}$.

2.3. The final phase

We only have AGB wind momentum and mass conservation in the final phase of evolution when the pressure of the hot bubble, $P \rightarrow 0$:

$$\begin{aligned} P_s &= \int_{R'}^{R_s} 4\pi r^2 \rho_{AGB} V dr + P' \\ &= \dot{M}(R_s - R') + P', \end{aligned} \quad (20)$$

$$\begin{aligned} M_s &= \int_{R'}^{R_s} 4\pi r^2 \rho_{AGB} dr + M' \\ &= \frac{\dot{M}}{V}(R_s - R') + M', \end{aligned} \quad (21)$$

where P' and M' are the momentum and mass acquired by the time the shell radius reaches some value R' . For the shell velocity we now have:

$$V_s = \frac{P_s}{M_s} = \frac{\dot{M}(R_s - R') + P'}{\dot{M}(R_s - R') + M'V} V \rightarrow V, \quad (22)$$

as $R_s \rightarrow \infty$.

During the early phases, the PN shell tends to the contact discontinuity, while in the last phase, it will be just behind the isothermal forward shock. If we apply isothermal shock jump conditions, we can estimate:

$$\rho_s = M^2 \rho_{AGB}, \quad (23)$$

where $M = V_s/c_s$ is the Mach number and c_s , the isothermal sound speed. The density jump is not limited to a maximum value of 4, as in an adiabatic shock. If $V_s \approx \text{const.}$, then $\rho \propto R_s^{-2}$ behind the shock.

3. Theoretical $\Sigma - D$ relation for PNe

Assuming a thermal bremsstrahlung mechanism is responsible for radiation of H II regions at radio wavelengths, we may write the volume emissivity ε_ν of a PN as:

$$\varepsilon_\nu [\text{ergs s}^{-1} \text{ cm}^{-3} \text{ Hz}^{-1}] \propto n^2 T^{-1/2}, \quad (24)$$

(Rohlfis & Wilson 1996) where n is the volume density and T the electron temperature.

The surface brightness can be expressed as:

$$\Sigma_\nu \propto \frac{L_\nu}{D^2} \propto \varepsilon_\nu D, \quad (25)$$

where L_ν is luminosity and $D = 2R_s$, the diameter of the PN. We combine Equations (24) and (25), use the derived dependence from Section 2 such that $n \propto \rho_s \propto D^{-1}$, and assume that temperature is constant.³ This radio surface brightness to diameter relation has a different form for the first and second phase of evolution (in comparison to the earlier result given in Paper I):

$$\Sigma \propto n^2 T^{-1/2} D \propto D^{-1}. \quad (26)$$

Generally, we may write $n \propto D^{-x}$, where $x \gtrsim 1$ (if $\Delta = \text{const.}$).

We do not expect the temperature to be strictly constant throughout the nebula. There are temperature gradients in PNe arising from radiation hardening. More energetic photons will travel further and when they are absorbed by the PN, they will impart a greater kinetic energy to the ions thereby producing a higher temperature. This would only slightly increase the value for β (+0.1 approximately), although the $T_e - D$ dependence is not quite of the power-law form (see numerical model results from Evans & Dopita 1985).

The value $\beta = 1$ under the above conditions (including $\Delta = \text{const.}$) is only a theoretical lower limit; the $\Sigma - D$

relation could be steeper due to these effects, as can be seen from Equation (26). The relation given here is derived under the assumption of spherical symmetric expansion. However, we know that the large number of PNe show a high asymmetry and can have a very complex morphology. This may explain why the theoretical $\Sigma - D$ relation is not necessarily connected to the empirical relations that we discuss in Section 4. Even if we had a spherically symmetric PNe with $\Sigma \propto D^{-1}$, the constant of proportionality would be different for different phases of evolution, as can be inferred from Section 2. Moreover, parameters governing the evolution (V , v , \dot{M} , \dot{m}) are not the same for all PNe, so no unique empirical relation for PNe is feasible.

In the final stage of evolution, after the fast wind has ceased, the isothermal shock wave continuously perturbs AGB wind. Nonetheless, the surface brightness steeply declines, as demonstrated in Paper I, because the mechanical energy input (acceleration) from the central star no longer exists. Using $\rho_{AGB} \propto R_s^{-2}$, the $\Sigma - D$ relation in the final stage of PN evolution can be expressed as:

$$\Sigma \propto D^{-3}. \quad (27)$$

4. The empirical $\Sigma - D$ relation for PNe

The most important prerequisite for defining a proper empirical $\Sigma - D$ relation is the extraction of a valid sample of PNe. This sample should consist of calibrators having well determined distances.

The distances to the calibrators have to be determined by reliable methods. These may include trigonometric or spectroscopic parallaxes of PN central stars and methods based on nebulae expansion. Although limited by current technology, trigonometric parallax is the most direct method of measuring distances.

All extracted PN samples suffer from severe selection effects caused by limitations in survey sensitivity and resolution. For Galactic samples, Malmquist bias⁴ may be the most severe effect; this is similar to the situation for Galactic SNR samples (Urošević et al. 2005).

For the literature extracted PN samples in this paper, we used flux densities at 5 GHz. This is because most PNe are expected to be optically thin at this frequency (see Section 5). Radio diameters would be preferable, however for most PNe used here, only optical diameters are available.

We extracted 27 PN sample sets as shown in Tables 1 and 2. While both detail fit parameters for $\Sigma - D$ and $L - D$, Table 1 does so by author (18 PN sets) and Table 2 by the specific distance determination method used (9 PN sets).

Data for sample Nos. 1 – 4 in Table 1 are taken from SSV and Cahn et al. (1992). We used Equation (7) from Van de Steene & Zijlstra (1995) to convert the brightness temperatures listed in Ph02 to their 5 GHz flux. PN distance ranges (kpc) are listed in Table 1 (e.g. “ $1.0 < d \leq$

⁴ Intrinsically bright PNe are favored in any flux limited survey because they are sampled from a larger spatial volume.

³ H II regions are approximately isothermal at $T \sim 10^4$ K.

2.0" indicates that all PNe in that set have distances between 1 and 2 kpc). Three PNe (He 1-5, HDW 6 and HaWe 5) indicated by "+" were removed from some sets because of inconsistencies with other data, as we will detail in Section 5.

Sample set 15 is taken from Zhang (1995) and consists of 132 PNe with well-determined individual distances. Set 16 contains 23 PNe with well-determined distances, while, set 17 consists of 132 Galactic bulge PNe. Both samples were taken from Van de Steene & Zijlstra (1995). Set 14 consists of 109 Galactic bulge PNe taken from Bensby & Lundström (2001). Set 18 (88 PNe) is actually the Van de Steene & Zijlstra (1995) Galactic bulge sample with stronger criteria applied to extract Galactic bulge PNe as defined in Bensby & Lundström (2001).

The first eight sample sets listed in Table 2 were obtained from SSV and Ph02 data. Set 9, USNO-PN, consists of PNe with well-measured trigonometric parallaxes, determined by United States Naval Observatory (USNO) ground based observations (Harris et al. 2007). Details of this USNO-PN sample data are presented in Table 3.

The trigonometric parallaxes of PNe determined by the Hipparcos mission suffer from large measurement errors (Harris et al. 2007) and therefore are of limited practical use for our study. The average measurement error in Hipparcos trigonometric parallaxes for some of our PNe is 57 %. Thus, the USNO-PN sample set is more reliable and have more accurate distance measurements⁵. The $\Sigma - D$ relation for the USNO-PN sample has the following form:

$$\Sigma = 7.39_{-2.79}^{+4.50} 10^{-22} D^{-2.38 \pm 0.56}. \quad (28)$$

Corresponding $\Sigma_\nu - D$ and $L_\nu - D$ diagrams are shown in Fig. 1.

Malmquist bias tends to increase the slope of the $\Sigma - D$ relation for SNRs (Urošević et al. 2005). Similar implications should be valid for PNe as well. Slopes from Table 1 suggest that some of our sample sets may suffer from a Malmquist bias. Specifically, $\Sigma - D$ slopes derived from the SSV and SSV+Ph02 are steeper for higher sampling distances (i.e. > 2 kpc).

In spite of the possibility of Malmquist bias, the majority of the $\Sigma - D$ slopes listed Tables 1 and 2, are very close to the so-called trivial $\Sigma - D$ relation with $\beta = 2$ (Arbutina et al. 2004). This can be understood mathematically from:

$$\Sigma \propto \frac{S}{\Omega} \propto \frac{L(D)/d^2}{D^2/d^2} \propto D^{-2} L(D), \quad (29)$$

where S is the flux density, Ω is the solid angle occupied by the source and d is the source distance. The usefulness of the $\Sigma - D$ relation can be tested with the correlation coefficient r_{L-D} of the $L - D$ relation, which should approach -1.0 if the data can be explained by a linear relation.

It is clear from Equation (29) that the $\Sigma - D$ relation has a trivial $\Sigma \propto D^{-2}$ form in the absence of $L - D$

correlation. The abundance of low r_{L-D} values as shown in Tables 1 and 2, indicate that the dependence between Σ and D is uncertain. Therefore, the validity of $\Sigma - D$ relations is diminished even if free from Malmquist bias. Aside from a few potential sample sets, including No. 1 listed in Table 1, most should not be used when calibrating the PN $\Sigma - D$ relation.

Sample No. 1 in Table 1 is the only set with a respectable correlation coefficient, $r_{L-D} = -0.67$, yet having a low probability of Malmquist bias⁶. This SSV sample consists of 13 relatively nearby Galactic PNe, with reliable individually determined distances less than 1 kpc. They are different in morphological form (e.g. round, elliptical, bipolar core, bipolar, etc.). For this sample, we obtain the $\Sigma - D$ relation:

$$\Sigma = 7.83_{-2.73}^{+4.17} 10^{-22} D^{-2.61 \pm 0.21}, \quad (30)$$

and a corresponding $\Sigma_\nu - D$ and $L_\nu - D$ diagrams are shown in Fig. 2.

We define the fractional error as:

$$fe = \left| \frac{d_{SSV} - d_\Sigma}{d_{SSV}} \right|, \quad (31)$$

in order to obtain an additional estimate of accuracy. Independently derived distances d_{SSV} are taken from SSV and d_Σ is the distance derived (for each individual PN) from the $\Sigma - D$ relation. The maximum and average fractional errors are $fe_{max} = 1.08$ and $\bar{fe} = 0.35$, respectively.

According to our criteria and the relatively small average fractional error, Equation (30) may be used as a calibration relation for distance determination. Since the PNe in the corresponding sample are nearby, the Malmquist bias should not be significant. The $L - D$ relation exists and the slope β is reasonable. However, this slope is still most likely a "mixture" of the evolutionary and selection effects. Additionally, the sample number is small (only 13 PNe) and they do not belong to the same morphological type. Therefore, all results obtained using Equation (30) should be taken with caution as we discuss below.

5. Discussion

In Section 2, we derived the theoretical dependence between the gas density in the PN shell and its radius with respect to the interacting stellar winds model. Next, we showed that the slope of the theoretical $\Sigma - D$ relation is changed significantly by including these equations.

The theoretically derived slope ($\beta \approx 1$) is shallower than slopes from the empirical relations given in Tables 1 and 2. This discrepancy may possibly be explained by poor quality of Galactic PN samples or by incorrect assumptions used for the derivation of the theoretical relation. Due to variations in the power law density distribution derived here and the approximately constant temperature of the expanding PN envelope, the theoretical

⁵ An average error of measured trigonometric parallaxes in this sample is 17.2 %.

⁶ The correlation coefficients for sets 3 and 9 from Table 1 are the steepest, but Malmquist bias is also likely. All other $\Sigma - D$ slopes are approximately trivial.

Table 1. The results of the $\Sigma - D$ and $L - D$ fits, where the parameters of the fit (β and α , respectively) and the correlation coefficient r are given for each sample. The number of PNe in the sample is given in the last column (N). SSV stands for Stanghellini, Shaw & Villaver (2008), B&L for Bensby & Lundström (2001) and Ph02 for Phillips (2002).

No.	Sample ^a	$\beta_{\Sigma-D}$	$r_{\Sigma-D}$	α_{L-D}	r_{L-D}	N
01	SSV $d < 1.0$	2.61±0.21	-0.97	0.61±0.21	-0.67	13
02	SSV $1.0 \leq d < 2.0$	1.89±0.43	-0.78	-0.11±0.43	0.08	15
03	SSV $d \geq 2.0$	3.96±0.62	-0.91	1.97±0.61	-0.73	11
04	SSV	2.56±0.22	-0.89	0.56±0.22	-0.40	39
05	SSV + Ph02 $d \leq 0.4$	1.47±0.40	-0.74	-0.53±0.40	0.38	13
06	SSV + Ph02 $0.4 < d \leq 0.6$	2.18±0.22	-0.91	0.18±0.22	-0.17	23
07	SSV + Ph02 $0.6 < d \leq 1.0$	2.37±0.20	-0.95	0.37±0.20	-0.43	18
08	SSV + Ph02 $1.0 < d \leq 2.0$	2.64±0.40	-0.88	0.64±0.40	-0.41	15
09	SSV + Ph02 $d > 2.0$	4.44±0.47	-0.96	2.44±0.47	-0.90	9
10	SSV + Ph02	2.40±0.17	-0.86	0.40±0.17	-0.27	78
11	SSV + Ph02 $d \leq 0.4$ †	2.31±0.38	-0.90	0.31±0.38	-0.26	11
12	SSV + Ph02 $0.4 < d \leq 0.6$ †	2.33±0.15	-0.96	0.33±0.15	-0.44	22
13	SSV + Ph02 †	2.57±0.14	-0.92	0.57±0.14	-0.45	75
14	B&L	2.31±0.11	-0.90	0.31±0.11	-0.26	109
15	Zhang (1995)	2.17±0.14	-0.80	0.17±0.14	-0.10	132
16	Van de Steene & Zijlstra (1995)	2.41±0.34	-0.84	0.41±0.34	-0.26	23
17	Van de Steene & Zijlstra (1995)	2.24±0.09	-0.92	0.24±0.09	-0.24	132
18	Van de Steene & Zijlstra (1995) (stronger criteria by B&L)	2.21±0.09	-0.94	0.21±0.09	-0.25	88

^aPNe from Ph02 are included in the sample sets (5 – 13) as additional, if they were not extracted by the SSV in their sample; $d < 1$ denotes that a set of PNe have distances less than 1 kpc, $1 \leq d < 2$, between 1 and 2 kpc, etc.

† – 3 PNe (He 1-5, HDW 6 and HaWe 5) are removed (see text).

Table 2. The results of the $\Sigma - D$ and $L - D$ fits of PN samples defined using the different methods of distance determination. The parameters of the fit (β and α , respectively) and the correlation coefficient r are given for each sample. The number of PNe in the sample is given in the last column (N).

No.	Sample ^a	$\beta_{\Sigma-D}$	$r_{\Sigma-D}$	α_{L-D}	r_{L-D}	N
1	Trigonometric Parallax	1.79±0.22	-0.90	-0.21 ±0.22	0.23	18
2	Trigonometric Parallax †	2.02±0.18	-0.95	0.02 ±0.18	-0.02	17
3	Geometrical (trig. parall. + expan.)	2.26±0.26	-0.86	0.26±0.26	-0.19	30
4	Geometrical (trig. parall. + expan.) †	2.44±0.22	-0.91	0.44±0.22	-0.36	29
5	Gravitational	1.42±0.37	-0.66	-0.58 ±0.37	0.33	22
6	Gravitational †	2.53±0.31	-0.89	0.53 ±0.31	-0.38	20
7	Spectroscopic	2.57±0.36	-0.91	0.57 ±0.36	-0.43	13
8	Extinction	1.69±0.38	-0.80	-0.31 ±0.38	0.25	13
9	USNO-PN	2.38±0.56	-0.90	0.38 ±0.56	-0.32	6

^a For the first eight samples, PNe are extracted from the SSV and Ph02; for USNO-PN – see Table 3.

Table 3. The data for the USNO PN sample.

Name	Trigonometric Parallax [mas]	$S_{5\text{GHz}}$ [mJy]	Diameter ["]
NGC 7293 (036.1-57.1)	4.56 ± 0.49	1292 ^a	660 ^b
NGC 6853 (060.8-03.6)	3.81 ± 0.47	1325 ^a	340 ^a
NGC 6720 (063.1+13.9)	1.42 ± 0.55	384 ^a	60 ^c
A 21 (205.1+14.2)	1.85 ± 0.51	157 ^d	550 ^e
A 7 (215.5-30.8)	1.48 ± 0.42	305 ^a	760 ^a
A 24 (217.1+14.7)	1.92 ± 0.34	36 ^a	415 ^d

References: ^aCahn et al. (1992); ^bO'Dell (1998); ^cGeorge et al. (1974); ^dHua & Kwok (1999); ^eSalter et al. (1984).

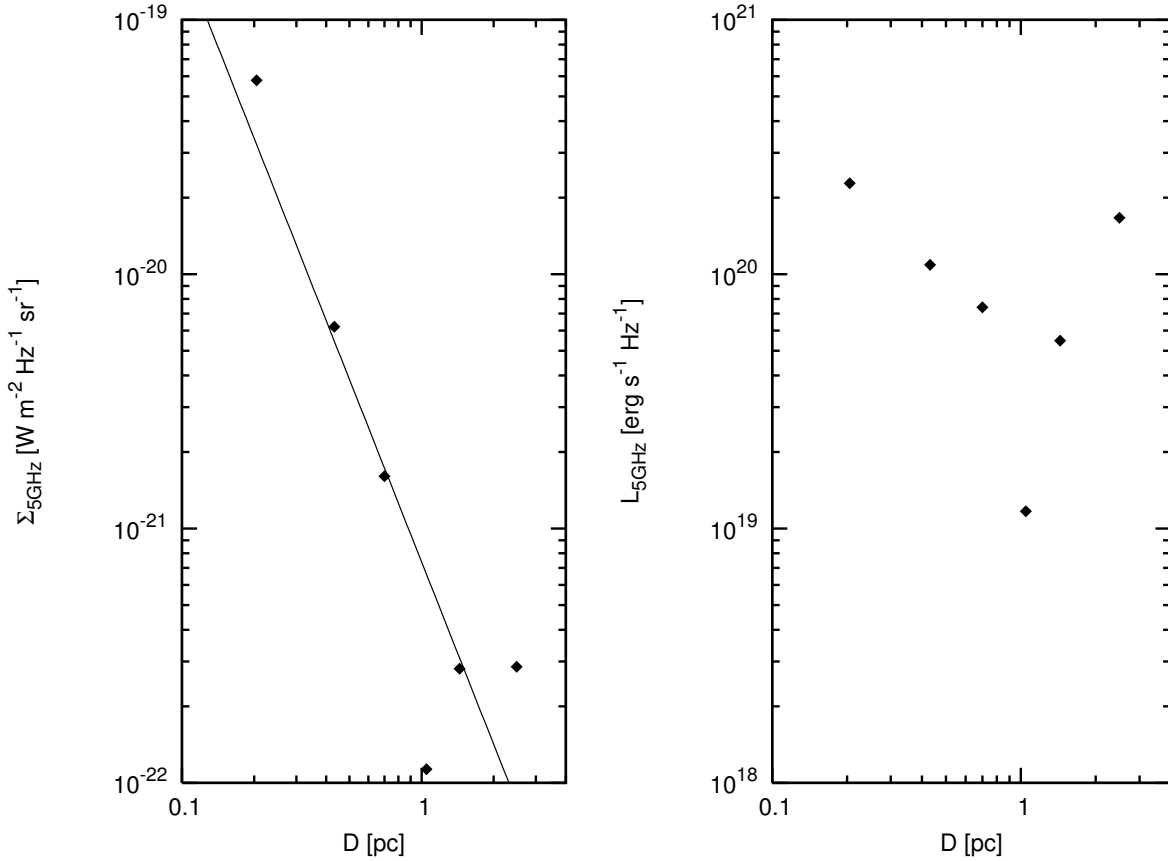


Fig. 1. (*Left*) $\Sigma_\nu - D$ diagram at 5 GHz for sample set 9 in Table 2, having 6 USNO-PNe with accurate trigonometric distances determinations. (*Right*) Corresponding 5 GHz $L_\nu - D$ diagram for the same set of PNe.

slope may be different than given in Equations (26) and (27) (derived assuming the shell thickness $\Delta \approx \text{const.}$). If the filling factor f is constant, the slope β could be as great as 3. We conclude that whether these simply derived theoretical relations have the correct forms or not, empirical relations are under the influence of biases that make their slopes different than they would be if one considers the evolution of a single hypothetical PN. An empirical relation can be useful for estimating distances only under strict conditions as discussed below.

Van de Steene & Zijlstra (1995) and Phillips (2004) showed that the evolution of PNe may not have a linear trend in log-log scales. When the radiation of the central star begins to ionize the nebula, the radio brightness will increase rapidly. However, in this phase of PN evolution, the observed incidence of radio nebulae is predicted to be low. Therefore, our linear trend of the $\Sigma - D$ form can be justified and the quadratic form of the $R - T_b$ dependence given by Phillips (2004) is not necessary for the statistical analysis given here. In addition, different dependencies can not be derived from the thermal bremsstrahlung radiation formula (Equation 24).

The subjects of our analysis are optically thin PNe. The reason for the low incidence of observed radio PN during the rising phase, discussed above, is that the majority of these PNe are optically thick at 5 GHz. Then, when the

central star reaches a temperature of 40 000 K, the number of ionizing photons becomes almost independent of temperature and radio luminosity no longer increases. As discussed by Van de Steene & Zijlstra (1995), this causes a decrease in surface brightness with a gradual expansion of the nebula, which then becomes optically thin and thus detectable. To keep our sample pure, we devised a set of criteria which excluded three suspected thick PNe in their rising phase of evolution (as marked with “†” in Table 1).

From Tables 1 and 2, we suggest that 24 slopes are most likely trivial $\Sigma - D$ relations. Therefore, we feel that the Malmquist bias is not so severe as in the case of Galactic SNR samples, where the slopes are significantly steeper. For example, the obtained slope for the sample of 132 bulge PNe collected by Van de Steene & Zijlstra (1995) takes a relatively shallow value of $\beta \approx 2$. This is expected result since all 132 PNe are located at the approximately same distance. Malmquist bias does not exist in samples which contain objects at the same distance.

Both Schneider & Buckley (1996) and at a later time, Bensby & Lundström (2001) attempted to improve the Bulge sample by removing foreground and background PNe. Bensby & Lundström (2001) defined stronger criteria to extract a more pure Bulge sample (Set 14 in Table 1). We found a trivial $\Sigma - D$ slope for this sam-

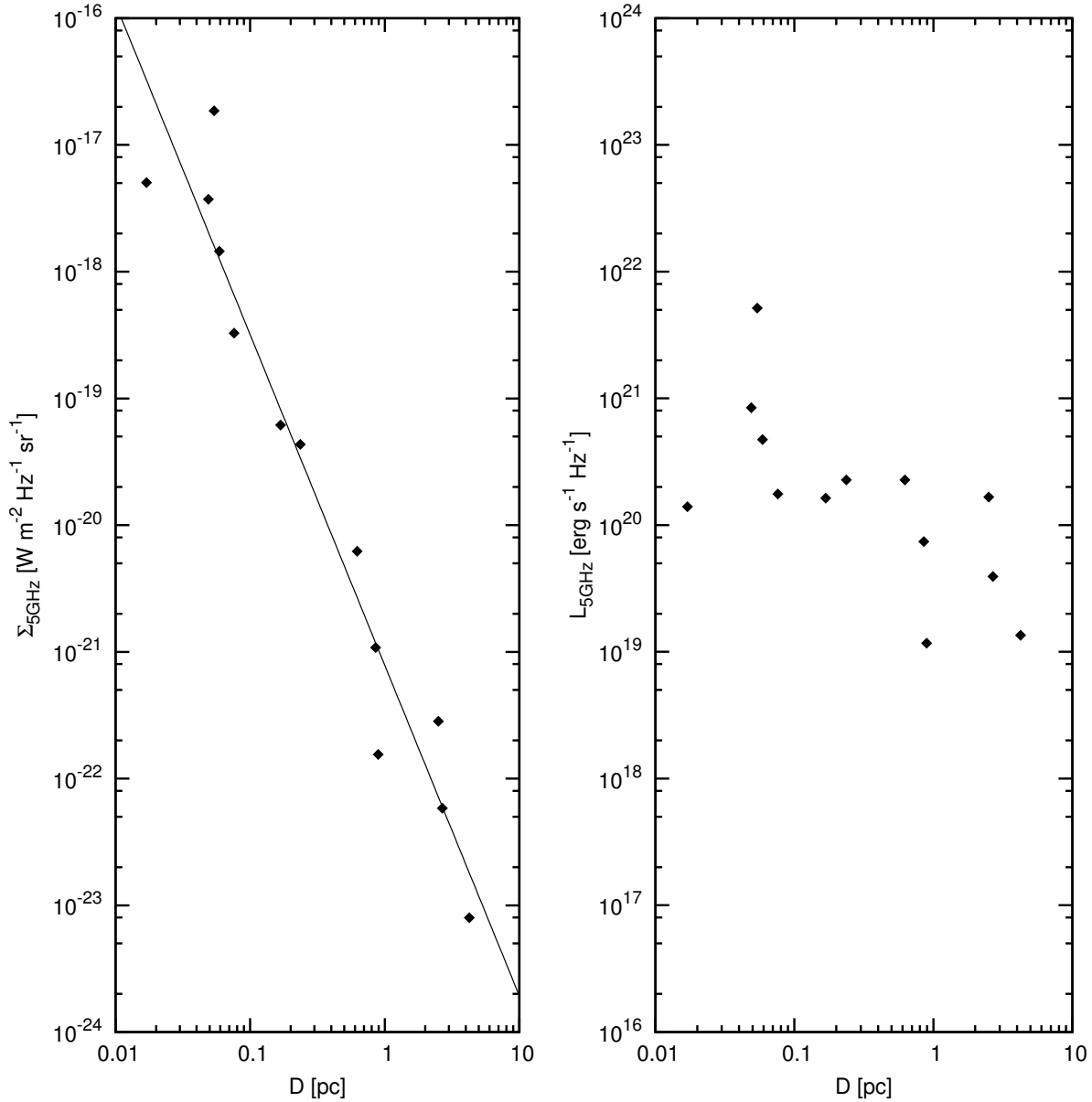


Fig. 2. (Left) $\Sigma_\nu - D$ diagram at 5 GHz for the set of 13 SSV PNe with distances < 1 kpc (from sample set 1 in Table 1). (Right) Corresponding $L_\nu - D$ diagram at 5 GHz for the same set of PNe.

ple. We also applied this stronger criteria directly to the Van de Steene & Zijlstra (1995) sample. The change in slope for this modified Van de Steene & Zijlstra sample (Set 18 in Table 1) is negligible. This again supports the idea that these sample sets are not strongly affected by the Malmquist bias.

According to criteria defined in this paper, the corresponding slopes for the Bulge samples represent the result of scattering in the $L - D$ plane. This slope ($\beta \approx 2$) was obtained for the extragalactic samples of SNRs (except M82 sample) where Malmquist bias also does not have severe effect. Again, this is because all of the SNRs in each set are at approximately the same distance (see Urošević 2002 and Urošević et al. 2005).

By examination of sample sets 5 – 9 in Table 1 (and Fig. 3) we try to demonstrate the effect of Malmquist bias. For set 5 with distances less than 0.4 kpc, the corresponding $\Sigma - D$ slope is $\beta = 1.47$. Further distance comparisons (in the form of distance interval in kpc followed by the $\Sigma - D$ slope) include: $0.4 < d \leq 0.6$, 2.18; $0.6 < d \leq 1.0$, 2.37; $1.0 < d \leq 2.0$, 2.64; and > 2.0 , 4.44. This implies that an increase in distance gives a $\Sigma - D$ slope that is also greater.

Using both the Tukey-Kramer (T-K) and the Scheffe (S) methods, we found the $\Sigma - D$ slope for sample set 9 in Table 1 (> 2.0 , 4.44) is statistically different at a confidence level of $\alpha = 0.05$, if compared to the slopes of sets 5, 6, and 7. However, since all of these samples consist of PNe with some uncertainty in their distances,

any firmer conclusion about their Malmquist bias should be avoided. Using the same methods, sets 1 (< 1 , 2.61) and 3 (≥ 2 , 3.96) in Table 1 also represent a statistically different population at a confidence level of $\alpha = 0.05$. The difference between their corresponding $\Sigma - D$ slopes is statistically significant at a confidence level of $\alpha = 0.2$ and can be explained by the Malmquist bias. Sample set 2 in Table 1 is omitted from our slope analysis because of its extremely high level of scattering in the $L - D$ plane (see Table 1, $r_{L-D} = 0.08$).

Inspection of Table 2 reveals that while all $\Sigma - D$ slopes are relatively close to the trivial form, set 4, 6 and 7 are a bit steeper. The increased slope of set 4 can be explained by perturbations induced by twelve very luminous and highly $\Sigma - D$ plane dispersed “expansion” PNe added to sample set 2. Since the gravitational and spectroscopic methods are mostly applied for distant PNe, slopes in sets 6 and 7 may be steeper due to a Malmquist bias. However, all of the $L - D$ correlation coefficients in Table 2 are very low and therefore poor for statistical investigations.

The high level of scattering in the $L - D$ plane, as seen in Figs. 1 (right) and 4, supports the idea that most of the slopes in Tables 1 and 2 do not have any real physical interpretation. It is this luminosity-diameter scattering artifact which produces the trivial $\Sigma \propto D^{-2}$ form. Therefore, 24 of these trivial $\Sigma - D$ slopes are not useful for the determination of distances. Causes for this scattering include: imprecisely determined calibrator distances, mixtures of different PN types in the same sample, limitations in sensitivity and resolution of radio surveys, source confusion and to a lesser extent, Malmquist bias.

Although, our criteria imply that the relation given in Equation (30) could be useful for distance determination, we assign a low confidence that it represents a real evolutionary track. The $\Sigma - D$ slope from this relation represents the result of coupling of evolutionary and selection effects. The corresponding sample set consist of only 13 PNe and they do not belong to the same morphological type. Thus, this sample is not complete or homogeneous and distance estimates obtained by using Equation (30) should be viewed with appropriate caution.

PN radio surface brightness depends on a number of factors that include: intrinsic nebula evolution, changes in density and temperature, changes in medium ionization and extremely large luminosity variations in the central star during its evolution. In Section 2, we assumed that shell expansion was constant throughout each phase of nebula evolution. On the contrary, PN shells are accelerated by the central star fast winds at the beginning of PN evolution, and only later are they driven at approximately constant speed by the hot bubbles created by the crossing of the fast winds through the inner shocks. Shaw et al. (2001) discusses acceleration of PN shells, i.e. how the velocity of PN shells is related to the evolution of the central star. They emphasized that the acceleration of shells is nearly zero in larger (and probably older) PNe having diameters > 0.03 pc. Almost all of the PNe from sample sets presented in Tables 1 and 2 are larger

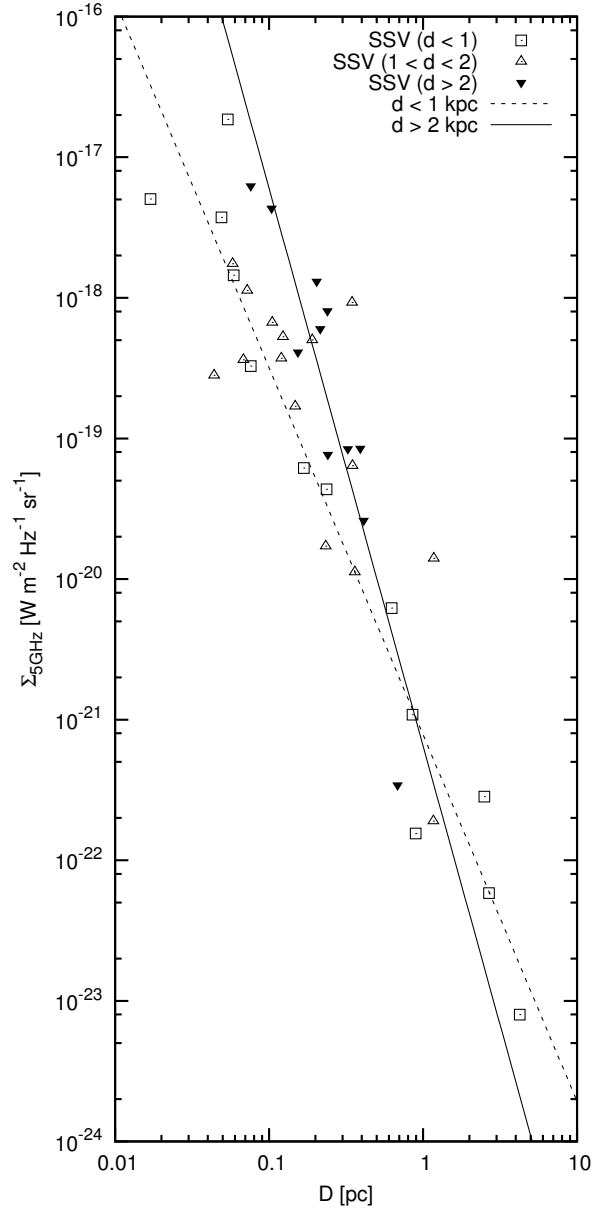


Fig. 3. The $\Sigma_\nu - D$ diagram at 5 GHz for all 39 SSV PNe (sample set 4) with reliable individually determined distances. The straight lines represent the least square fit lines through the two distance limiting Galactic samples. The difference in slope of corresponding $\Sigma - D$ relations are defined for PNe with distances < 1 kpc and ≥ 2 kpc (represented with dash and tick line, respectively). These could be explained as a result of the volume selection effect called Malmquist bias.

than 0.03 pc (see Fig. 4) and therefore in later phases of evolution where acceleration (or central star influence) is negligible. This explanation is admittedly simplistic. For essential understanding of the theoretical and empirical $\Sigma - D$ dependencies, the full explanation of the complex co-evolution of a nebula and its central star would be needed.

The most massive central stars will never fully ionize their environment and those PNe will never become optically thin at 5 GHz since their central stars evolve so rapidly. Those observed PNe with smaller diameters and surface brightnesses (optically thick PNe at 5 GHz) are located significantly lower in the $\Sigma - D$ or $L - D$ planes when compared to the average (thin) PNe. Their evolution are surely not defined by the $\Sigma - D$ relations derived here. Although the majority of the thick PNe will become thin, the question is WHEN? This depends on a number of factors during their evolution. These effects significantly contribute to uncertainties in addition to the huge scattering found in the $L - D$ plane.

Other factors not included in our analysis may have a large impact on the evolution of PN emissivity. These include: compression of gas induced by the interaction of fast wind with the medium on the main shell inner boundary, isothermal shocks associated with the passage of D-ionization fronts through neutral gas and progressive ionization of greater amounts of surrounding neutral gas (e.g. Shaw et al. 2006, and references therein). We do not analyze ionization fronts in this paper; our derivations in Section 2 are based only on the dynamics of corresponding shock waves. The surface brightness evolution may be more closely connected to ionization than the dynamical expansion of the shell. This may be good enough reason to challenge the quality of our derived theoretical relations and an additional explanation for scattering in the $L - D$ plane. Finally, we concede that some PNe could have different initial conditions leading to independent evolutionary paths. These paths could follow the same theoretical $\Sigma - D$ curve but with varying intercepts, therefore leading to the observed scatter.

In order to define a valid PN sample for statistical investigation, one needs to separate a higher number of nearby PNe with the same morphological characteristics. We define such a sample (USNO-PN) in the subsection below (Section 5.1). However, the quality of radio-continuum observations today simply is not sensitive enough to provide a high number of similar PNe having reliably determined distances.

5.1. The USNO-PN Sample

We have examined the morphological properties of PNe from the USNO-PN sample using the radio images of these objects found in the literature. We use comparisons with radio morphological classes given by Aaquist & Kwok (1996) which are based on the *prolate ellipsoidal model* (PES). The PES model describes divergence in observed (empirical) morphologies through different sky projections of relatively simple spherical shell models with both radial and latitude density gradients and with different ionization depths. USNO-PN sample objects can be classified as follows: circular (NGC 7293 or Helix Nebula, see Zijlstra et al. 1989); open elliptical (NGC 6853 or Dumbbell Nebula, see Bignell 1983); elliptical

(NGC 6720 or Ring Nebula, see George et al. 1974); symmetric (A21 or S274, see Salter et al. 1984); and S-type (A24⁷). However, a further search of the literature reveals that the intrinsic morphologies for all five of these objects is most likely to be bipolar, i.e. that the structures of the emitting regions (or shells) range from a thick disk (Helix Nebula) to a triaxial ellipsoid (A24, and Ring Nebula) to a barrel-like shape (A21, and Dumbbell Nebula) (see O’Dell 1998, Henry et al. 1999, Hua & Kwok 1999, O’Dell et al. 2007 and Meaburn et al. 2000). The sixth object for which we found reliable radio observations (A7) appears to be a “classical” PN with a well defined spherical shell (Xilouris et al. 1996).

We note that Kastner et al. (1996) and Zuckerman & Gatley (1988) detected a shock-excited H₂ emission from the Helix, Ring and Dumbbell nebulae, implying an ionization bounded case for these objects. Additionally, no spectroscopic evidence for the existence of a high-velocity stellar wind has been found for the previously mentioned objects, including A7 (Cerruti-Sola & Perinotto 1985, Patriarchi & Perinotto 1991). Central stars of these objects are most likely well pass the hydrogen-shell burning phase and approaching the white dwarf cooling sequence.

A wide range of shell structures is predicted in the hydrodynamical models based on the ISW model and it is very likely that a large number of PNe classified by apparent morphology as spherical or elliptical, may in fact possess a bipolar structure. Even though morphological classifications based on optical imaging favor elliptical objects, Zuckerman & Aller (1986) predict that approximately 50% of all PN in the Galaxy are actually bipolar. Nevertheless, we conclude that the USNO-PN sample is not representative of the majority of PNe because of its “narrowness” in morphology (i.e. almost all appear to be bipolar).

6. Summary

The main results of this paper may be summarized as follows:

- (i) We have derived a new theoretical $\Sigma - D$ relation for PNe in the form $\Sigma \propto D^{-1}$ by including the interaction between the AGB star wind and the fast wind from the central star. This dependence is obtained for both momentum conserving and energy conserving phases of evolution. Only for the final stage, we did derive the same theoretical dependence ($\Sigma \propto D^{-3}$) as in Paper I.
- (ii) We derived empirical $\Sigma - D$ relations for 6 updated PN samples from the literature, 12 new sample sets extracted from these and 9 additional sets as defined in this paper. We discuss the selection effects that influence these PN sample sets. Our results show that

⁷ For A24 we acquire a 1.4 GHz radio image from the NRAO VLA Sky Survey (NVSS) postage stamp server (<http://www.cv.nrao.edu/nvss/postage.shtml>).

updated Galactic PN samples do not severely suffer from volume selection effects, i.e. Malmquist bias (similar as in case of the extragalactic SNR samples). We do note that the $\Sigma - D$ slope does increase with sample distance, possibly due to Malmquist bias as shown on two statistically different SSV samples with distance limits < 1 and ≥ 2 kpc. Because of this trend, we feel that samples consisting only of nearby PNe are useful for future statistical analysis.

- (iii) From the analysis of $L - D$ dependencies presented here, we conclude that 24 empirical $\Sigma - D$ relations (listed in Tables 1 and 2) for Galactic PNe should not be used to determine distances to other observed PNe or to establish any other PN evolutionary paths. These relations represent only a general trend of changes in surface brightness. Two obtained steep $\Sigma - D$ slopes for distant samples ($d > 2$ kpc) are probably the result of Malmquist bias. However, we extracted one useful nearby SSV subsample ($d < 1$ kpc, set 1 in Table 1). This updated sample consists of PNe with reliable and individually determined distances. A reasonable $L - D$ dependence does exist for this nearby sample. Since this sample consists of only 13 morphologically different PNe, the corresponding $\Sigma - D$ relation for distance determination must be used with caution.

Acknowledgements. We thank an anonymous referee for many helpful comments that substantially improved the quality of this paper. The authors thank Jeffrey Payne for careful reading and correction of the manuscript. This research has made use of the SIMBAD database operated at CDS in Strasbourg, France, NASA's Astrophysics Data System and has been supported by the Ministry of Science and Environmental Protection of the Republic of Serbia (Projects: Nos. 146002, 146003, and 146012).

References

- Aaquist, O. B., & Kwok, S. 1996, ApJ, 462, 813
 Amnuel, P.R., Guseinov, O.H., Novruzova, H.I. & Rustamov, Y.U.S. 1984, Ap&SS, 107, 19
 Arbutina, B., Urošević, D., Stanković, M. & Tešić, Lj. 2004, MNRAS, 350, 346
 Bensby, T. & Lundström, I. 2001, A&A, 374, 599
 Bignell, R. C. 1983, Planetary Nebulae, IAUS, 103, 69
 Cahn, J. H., Kaler, J. B. & Stanghellini, L. 1992, A&AS, 94, 399
 Cerruti-Sola, M., & Perinotto, M. 1985, ApJ, 291, 237
 Daub, C.T. 1982, ApJ, 260, 612
 Evans, I.N. & Dopita, M.A. 1985, ApJS, 58, 125
 George, D., Hartsuijker, A. P., & Kaftan-Kassim, M. A. 1974, A&A, 35, 219
 Harris, H.C. et al. 2007, AJ, 133, 631
 Henry, R. B. C., Kwitter, K. B., & Dufour, R. J. 1999, ApJ, 517, 782
 Hua, C. T., & Kwok, S. 1999, A&AS, 138, 275
 Kastner, J. H., Weintraub, D. A., Gatley, I., Merrill, K. M., & Probst, R. G. 1996, ApJ, 462, 777
 Kwok, S. 1994, PASP, 106, 344

- Kwok, S. 2000, The Origin and Evolution of Planetary Nebulae, Cambridge University Press
 Meaburn, J., Boumis, P., Christopoulou, P. E., Goudis, C. D., Bryce, M., & López, J. A. 2005, Revista Mexicana de Astronomia y Astrofisica, 41, 109
 O'Dell, C. R. 1998, AJ, 116, 1346
 O'Dell, C. R., Sabbadin, F., & Henney, W. J. 2007, AJ, 134, 1679
 Patriarchi, P., & Perinotto, M. 1991, A&AS, 91, 325
 Phillips, J.P. 2002, ApJS, 139, 199 (Ph02)
 Phillips, J.P. 2004, MNRAS, 353, 589
 Rohlfs, K. & Wilson, T.L. 1996, Tools of Radio Astronomy, Springer
 Salter, C. J., Greve, A., Weiler, K. W., Birkle, K., & Dennefeld, M. 1984, A&A, 137, 291
 Schneider, S.E. & Buckley, D. 1996, ApJ, 459, 606
 Stanghellini, L., Shaw, R.A. & Villaver, E. 2008, ApJ, 689, 194 (SSV)
 Shaw, R.A., Stanghellini, L., Mutchler, M., Balick, B. & Blades, J.C. 2001, ApJ, 548, 727
 Shaw, R.A., Stanghellini, L., Villaver, E. & Mutchler, M. 2006, ApJS, 167, 201
 Urošević, D. 2002, Serb. Astron. J., 165, 27
 Urošević, D., Pannuti, T. G., Duric, N. & Theodorou, A. 2005, A&A, 435, 437
 Urošević, D., Vukotić, B., Arbutina, B. & Ilić, D. 2007, Serb. Astron. J., 174, 73 (Paper I)
 Van de Steene, G.C. & Zijlstra, A.A. 1995, A&A, 293, 541
 Xilouris, K. M., Papamastorakis, J., Paleologou, E., & Terzian, Y. 1996, A&A, 310, 603
 Zhang, C.Y. & Kwok, S. 1993, ApJS, 88, 137
 Zhang, C.Y. 1995, ApJS, 98, 659
 Zijlstra, A. A., Pottasch, S. R., & Bignell, C. 1989, A&AS, 79, 329
 Zuckerman, B., & Aller, L. H. 1986, ApJ, 301, 772
 Zuckerman, B., & Gatley, I. 1988, ApJ, 324, 501

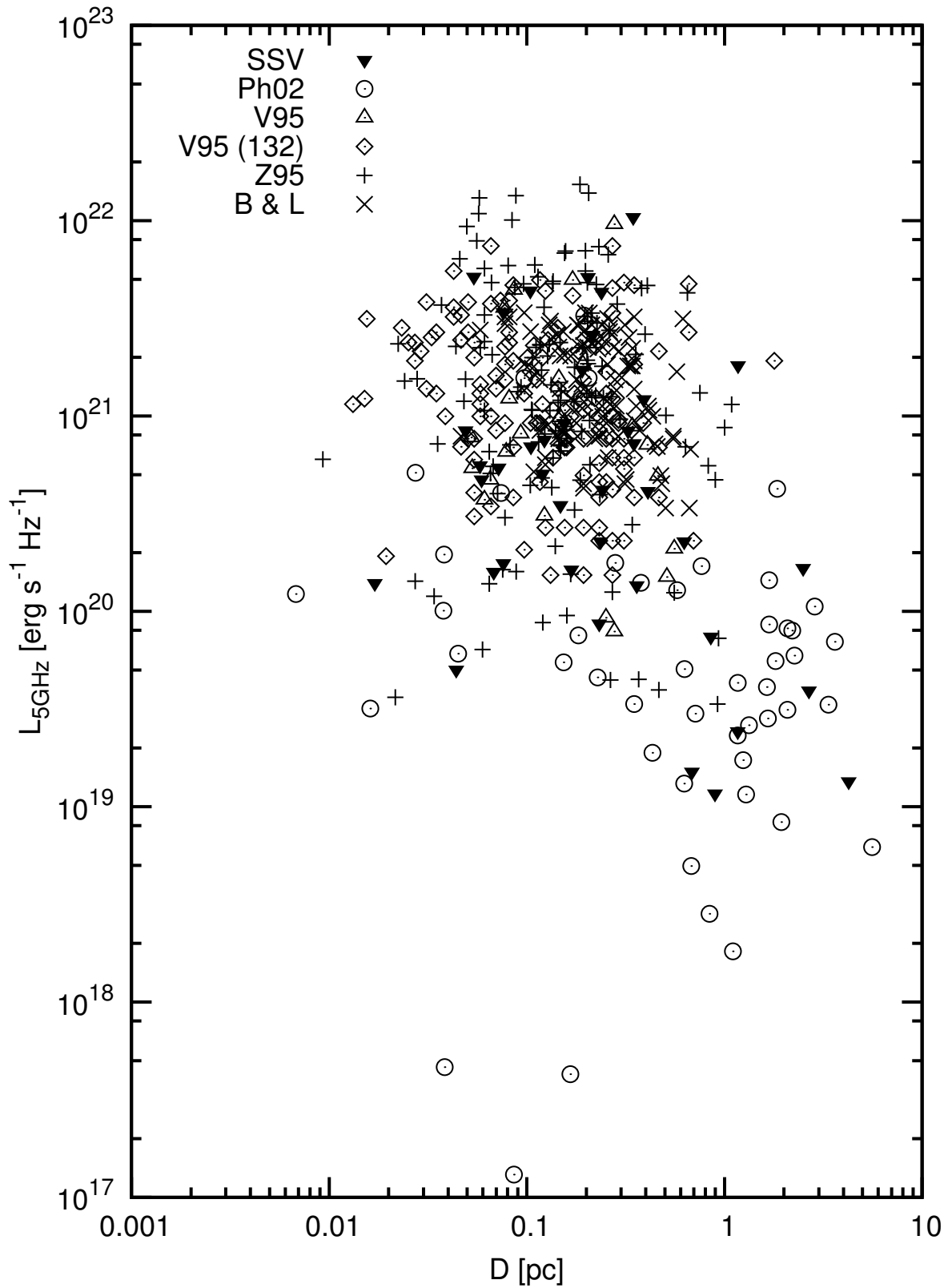


Fig. 4. The $L_\nu - D$ diagram for the samples of PNe given in Table 1.